An Optical Waveguide Study on the Nanopore Formation in Block Copolymer/Homopolymer Thin Films by Selective Solvent Swelling

Dong Ha Kim,*,†,‡ King Hang Aaron Lau,† Wonchul Joo,§ Juan Peng,† Unyong Jeong,± Craig J. Hawker,# Jin Kon Kim,*,§ Thomas P. Russell,*,⊥ and Wolfgang Knoll*,†

Max Planck Institute for Polymer Research, Ackermannweg 10, 55128 Mainz, Germany, Division of Nano Sciences and Department of Chemistry, Ewha Womans University, 11-1 Daehyun-dong, Seodaemun-gu, 120-750 Seoul, Korea, National Creative Research Initiative Center for Block Copolymer Self-Assembly, Department of Chemical Engineering and Polymer Research Institute, Pohang University of Science and Technology, Hyoja-dong, San 31, Nam-gu, Pohang, Kyungbuk 790-784, Korea, Materials Research Laboratory, University of California at Santa Barbara, Santa Barbara, California 93106, Silvio O. Conte National Center for Polymer Research, Polymer Science and Engineering Department, University of Massachusetts at Amherst, Amherst, Massachusetts 01003, and Department of Materials Science and Engineering, Yonsei University, 134 Shinchon-dong, Seoul 120-749, Korea

Received: May 18, 2006; In Final Form: June 14, 2006

Thin films of mixtures of asymmetric poly(styrene-*block*-methyl methacrylate) (PS-*b*-PMMA) diblock copolymers and PMMA homopolymers with cylindrical PMMA microdomains oriented normal to the substrate surface were used to couple optical modes in the Kretschmann configuration, and their optical properties were investigated by optical waveguide spectroscopy (OWS). The nanopore formation in the block copolymer (BCP) waveguide layer via selective solvent swelling and subsequent reannealing was monitored in terms of shifts in the coupling mode angles. The sequential swelling/reannealing of the initial mixture film resulted in a number of discrete or partially interconnected pores instead of cylindrical pores with a high aspect ratio. The simultaneous processes occurring inside and on top of the BCP waveguide layer were discerned independently with high selectivity for *p*- and *s*-polarization.

Introduction

Self-assembly has attracted increasing attention as a platform toward well-defined, ordered complex structures on the nanometer scale. In particular, block copolymers (BCPs) offer a significant potential as nanomaterials since they self-organize to form well-ordered, periodic nanoscale morphologies depending on the relative volume fraction of the constituent blocks.[1−6] There have been numerous efforts to use self-assembled BCPs as templates or scaffolds for the fabrication of functional nanostructures,[7−15] for instance, photonic band gap materials,[16] etching masks,[17] scaffolds for magnetic storage media,[18] and an increasing number of novel nanomaterials are being reported from this unique class of polymers.

In particular, thin films of diblock copolymers with cylindrical microdomains oriented normal to the surface are attractive due to the tunability of large aspect ratios of the cylindrical microdomains. Poly(styrene-*block*-methyl methacrylate) diblock copolymers (PS-*b*-PMMA) with cylindrical PMMA microdomains aligned normal to the surface constitute a typical example of such ordered nanostructures,[19] in which PMMA microdomains can be selectively etched away by deep UV exposure, leading to porous templates.[20]

Recently, Jeong et al. reported that thin films of PS-*b*-PMMA/PMMA homopolymer mixtures offer a novel route by which an array of high aspect ratio cylindrical pores with multiple length scales could be generated by either extracting the homopolymers using a selective solvent or removing the entire cylindrical microdomains via UV exposure followed by solvent rinsing.[21−24] The simple addition of a PMMA homopolymer to an asymmetric PS-*b*-PMMA was shown to markedly promote the orientation of nanodomains normal to the surface, enabling a directed self-assembly of the copolymers into arrays of highly oriented microdomains without applying an external electric field.[24]

An alternative route to fabricate nanoporous templates has been suggested by simple swelling of the cylindrical PMMA microdomains of the PS-*b*-PMMA film with smaller thicknesses by using an acetic acid, a preferential solvent for PMMA, at a temperature below the glass-transition temperature (T_g) of the two blocks.[25,26] Annealing the swollen block copolymer film above the T_g resulted in a recovery of the initial film morphology; thus, generated nanopores disappeared. Such a reversible process of solvent-induced reconstruction of the film was investigated by atomic force microscopy,[25] X-ray photoelectron spectroscopy,[26] and grazing incidence small-angle X-ray scattering experiments.[25]

In this article, the selective etching and subsequent annealing of thin films of mixtures of asymmetric PS-*b*-PMMA with cylindrical PMMA microdomains and PMMA homopolymers in which PMMA microdomains oriented normal to the film surface were employed to produce nanoporous thin films with arrays of discrete pores. The films served as planar waveguide layers in the experimental setup known as Kretschmann prism

* Corresponding authors. Tel.: +82-2-3277-4517. Fax: +82-2-3277-3419. E-mail: dhkim@ewha.ac.kr (D.H.K.); jkkim@postech.ac.kr (J.K.K.); russell@mail.pse.umass.edu (T.P.R.); and knoll@mpip-mainz.mpg.de (W.K.).
† Max Planck Institute for Polymer Research.
‡ Ewha Womans University.
§ Pohang University of Science and Technology.
± Yonsei University.
University of California at Santa Barbara.
⊥ University of Massachusetts at Amherst.

10.1021/jp0630469 CCC: $33.50 © 2006 American Chemical Society
Published on Web 07/19/2006

coupling configuration.[27,28] The structural changes in the thin films during swelling with a selective solvent for the PMMA blocks (without UV exposure) and subsequent reannealing process at high temperature were investigated by optical waveguide spectroscopy (OWS).[27−30] For comparison, we already reported an unprecedented application of thin films of mixtures of PS-*b*-PMMA/PMMA homopolymers with controlled nanodomain orientations as optical elements (i.e., planar waveguide layers).[31] Pore generation by removal of the entire PMMA domains and filling the nanopores with liquid media were successfully monitored by OWS. Unlike this previous study, we herein report a different route to quasi-reversible nanostructures with capped nanopores obtained from sequential selective swelling and reannealing processes. Specifically, the change in porous morphology occurring simultaneously inside and on top of the film was detected independently by monitoring guided optical modes under *p*- and *s*-polarization conditions.

Experimental Procedures

Materials. Commercial glass plates (LaSFN9, Schott Glass GmbH, $n = 1.85$ at $\lambda = 633$ nm) were used as substrates. 3-Mercaptopropyltrimethoxysilane (3-MPS) and tetramethoxysilane (TMOS) were purchased from Lancaster Synthesis GmbH and Fluka GmbH, respectively. Asymmetric diblock copolymers of polystyrene and poly(methyl methacrylate) (PS-*b*-PMMA) with an average molecular weight of 55 500 g/mol and a polydispersity of 1.19 were prepared by atom transfer radical polymerization as described previously.[33] The volume fraction of PMMA was $\phi = 0.3$. Atactic PMMA homopolymers with $M_w = 23\,600$ g/mol were purchased from Polymer Source, Inc. A hydroxy end-functionalized random copolymer of styrene and methyl methacrylate, denoted P(S-*r*-MMA), having a styrene fraction of $\phi = 0.6$, was synthesized in bulk via a nitroxide mediated living free radical polymerization.[19,33] The molecular weight was 9 600 g/mol with a polydispersity of 1.20 measured by size-exclusion chromatography.

Optical Waveguide Spectroscopy (OWS). We performed OWS experiments based on the Kretschmann prism coupling technique.[27] A home-built surface plasmon resonance (SPR) based optical detection setup was used. A HeNe laser (5 mW, Uniphase) beam passed through a chopper that was connected to a lock-in amplifier (EG&G). A polarizer (Glan-Thompson) for either *p*- or *s*-polarization was used. The substrate containing the waveguide layer was attached to the prism base with an index-matching oil. Consequently, the glass prism and the substrate formed an optically continuous medium. The incident laser was reflected off the base plane of the coupling prism, and the reflected intensity focused by a lens (L2, $f = 50$ mm, Ovis) was collected by a photodiode. The sample was mounted onto a two-phase goniometer (Huber) that could be moved in 0.001° steps operated by the connected personal computer.

To observe optical waveguide modes, the reflectivity (R) was measured as a function of the angle of incidence. Both transverse electric (TE) and transverse magnetic (TM) modes (corresponding to *s*- and *p*-polarizations, respectively) can be excited in the waveguide layers. At angles above θ_c, the critical angle for total internal reflection, guided modes can be observed as very sharp minima, indexed according to the number of nodes in their field distributions (e.g., $m = 0, 1, 2$, etc.). The angles for these modes are completely dictated by the dielectric properties (ϵ) and the thicknesses (h) of the waveguide layers (i.e., the glass coupling medium, the coupling gap metal layers, the primer layers, the waveguide layer, and the dielectric medium). Fresnel calculations were performed using the WINSPALL software (version 2.20) developed in the Max Planck Institute for Polymer Research in Germany.

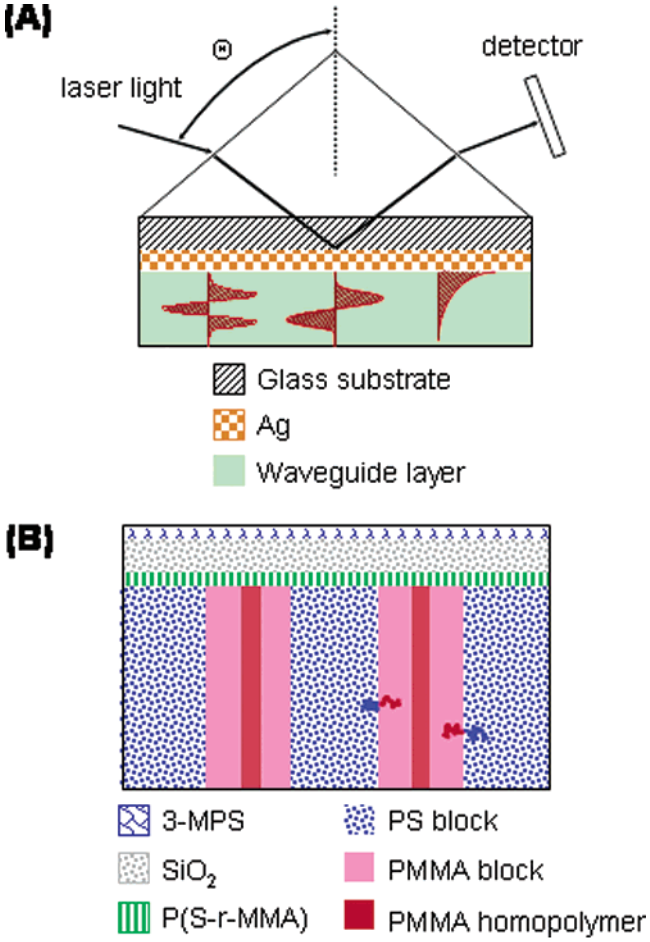

Figure 1. (A) Schematic diagram of the OWS setup based on the Kretschmann configuration and of the idealized field distributions of several guided modes (LaSFN9 glass/Cr/Ag/waveguide layer/air). (B) Detailed description of the waveguide layer in Figure 1A. Thin films of PS-*b*-PMMA and PMMA homopolymer mixture with PMMA cylindrical nanodomains aligned normal to the substrate surface were fabricated onto glass substrates via coupling gap layers.

Fabrication of Block Copolymer Films on Glass Substrates. Figure 1 shows the scheme of the Kretschmann prism coupling geometry containing block copolymer thin films. A LaSFN9 glass substrate was cleaned carefully with ultrasonication in a 1% detergent solution (HellmanexII, Hellma GmbH & Co.) and rinsed with Milli-Q water to remove any residue. A silver (Ag) substrate was prepared on glass substrates to excite surface plasmons between the metal and the underlying waveguide layer. Chromium (Cr, ∼2 nm) and silver (Ag, ∼50 nm) layers were deposited by thermal evaporation (Edwards, FL400) at a base pressure of 10^{-6} mbar. 3-MPS was then introduced as an adhesion-promoting layer between the Ag and the following silicon dioxide (SiO_2) layer. Evaporated Ag surfaces were immersed in 20 mM 3-MPS (previously vacuum distilled) in dry ethanol for 2 h to allow for the formation of self-assembled monolayers of nonpolymerized 3-MPS. The surfaces were then rinsed with copious amounts of dry ethanol and Milli-Q H_2O. Hydrolysis and condensation of the 3-MPS layers were performed in 0.1 M HCl for 1 h. The Ag surfaces were removed from the HCl solution after the 3-MPS condensation and rinsed with H_2O.

Silicon dioxide (SiO_2) substrates were prepared by a sol−gel process as reported previously.[34] Tetramethoxysilane (TMOS)

was delivered into a premixed solution of methanol, water, and 0.1 M HCl. A typical precursor solution for SiO_2 is composed of 163 μL of H_2O, 55 μL of methanol, 81 μL of 0.1 M HCl, and 20 μL of TMOS. The solution was shaken for ~30 min to facilitate TMOS hydrolysis prior to deposition. The hydrolyzed solution was delivered to the 3-MPS-modified Ag surface, and the sample was spun at ~3400 rpm for 1 min. The Ag/3-MPS/SiO_2 surface was stored in a desiccator at room temperature for a minimum of 2 days to complete the condensation process and to remove any residual solvent.

An energetically neutral surface for PS-*b*-PMMA films was then anchored to the SiO_2 layer using P(S-*r*-MMA) via the covalent coupling between the hydroxyl groups and the SiO_2 surface. The P(S-*r*-MMA) was spin-coated onto the SiO_2 surface from a 2% toluene solution at 1000 rpm followed by annealing under vacuum at 165 °C for 3 days. After rinsing with toluene, a well-defined layer of P(S-*r*-MMA) remained. The consecutive deposition of the coupling gap layers (i.e., 3-MPS/SiO_2/P(S-*r*-MMA) onto the Ag substrate was monitored separately by surface plasmon resonance (SPR) spectroscopy (see Figure S1 in the Supporting Information).

Thin films composed of PS-*b*-PMMA and PMMA homopolymer mixtures, containing 25 wt % PMMA homopolymers with respect to the amount of the PMMA block, were prepared by spin-coating 5 wt % toluene solutions at 500 rpm onto the P(S-*r*-MMA) surface. The films were annealed at 155 °C for 2 days under vacuum and then quenched to room temperature. The surface of a PS-*b*-PMMA/PMMA film fabricated onto such a modified glass substrate was examined by atomic force microscopy (AFM) (see Figure S2 in the Supporting Information). Hexagonally packed arrays of cylindrical PMMA microdomains oriented normal to the substrate are evident over a wide area of the film. The average center-to-center distance (λ_{C-C}) between PMMA microdomains was ~46 nm.

Microscopy. Atomic force microscopy (AFM) images were obtained using a Digital Instruments Dimension 3100 scanning force microscope in the tapping mode. Etched silicon tips on a cantilever (Nanoprobe) with spring constants ranging between 40.0 and 66.0 N/m were used. Field emission scanning electron microscopy (FESEM) images were obtained on field emission SEM (LEO 1530 Gemini) under 1 kV accelerating voltage. Transmission electron microscopy (TEM: Hitachi-7600) images were obtained under 100 kV accelerating voltage. Block copolymers coated on silicon wafers with a 200 nm thick sacrificial layer of SiO_2 were floated onto the surface of a 5 wt % HF solution and transferred to a copper grid. PS phases were selectively stained by RuO_4.

Results and Discussion

The overall procedure for the generation of nanopores in the BCP film by selective solvent swelling and subsequent annealing is schematically illustrated in Figure 2. Figure 2A shows the initial thin film of the PS-*b*-PMMA/PMMA homopolymer with cylindrical PMMA microdomains (M) oriented normal to the substrate, with PMMA homopolymers being located at the center of the PMMA microdomains. The PMMA domains slightly protrude from the PS surface by ~1 nm, as evidenced by the height contrast AFM image (Figure S2). The film was then immersed in acetic acid, a selective solvent for the minor component, PMMA. The PMMA homopolymer was extracted from the film, while the PMMA block chains near the film/air interface can migrate to the surface as depicted in Figure 2B. This process is essentially different from the previous studies on pore generation via UV degradation followed by solvent rinsing or selective solvent swelling for the neat block copolymer thin film itself.[25,26,31] Annealing above the glass-transition temperature (T_g) of the block copolymer results in a recovery of the migrated PMMA block chains near the film/air interface to the initial configuration, due to higher mobility at the air interface, capping the top of the individual nanopores. However, most preformed nanopores inside the film are partially covered by PMMA block chains as a result of relaxation and rearrangement, leaving behind permanent pores with a shape of a number of small strings of bubbles along the cylinder axis, as depicted in Figure 2C. Here, it is noteworthy that the individual capped nanopores by migrated PMMA block chains could open again to have nanopores at the air/film interface once selective solvent swelling is performed.

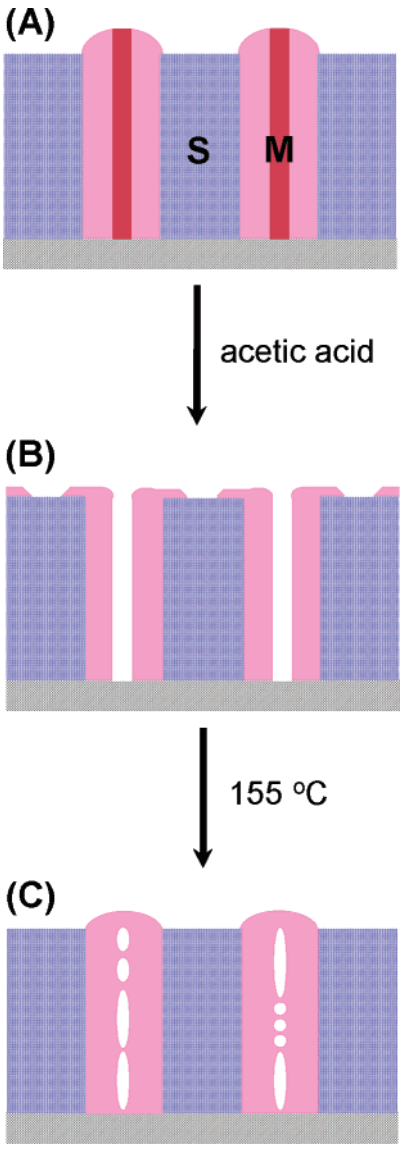

Figure 2. Schematic cross-sectional representation of the nanopore formation in PS-*b*-PMMA/PMMA film by selective solvent swelling: (A) PS-*b*-PMMA/PMMA mixture film with an array of cylindrical PMMA nanodomains oriented normal to the substrate surface; (B) identical film after immersion in acetic acid, a selective solvent for the PMMA component; and (C) identical film after immersion in acetic acid followed by annealing at 155 °C for 2 days under vacuum.

The surface morphologies of the BCP film for each step described in Figure 2A−C were investigated by topographical AFM study. Figure 3A is the height contrast AFM image (magnified as compared to the AFM image over a larger area in Figure S2) of the initial film as sketched in Figure 2A. The

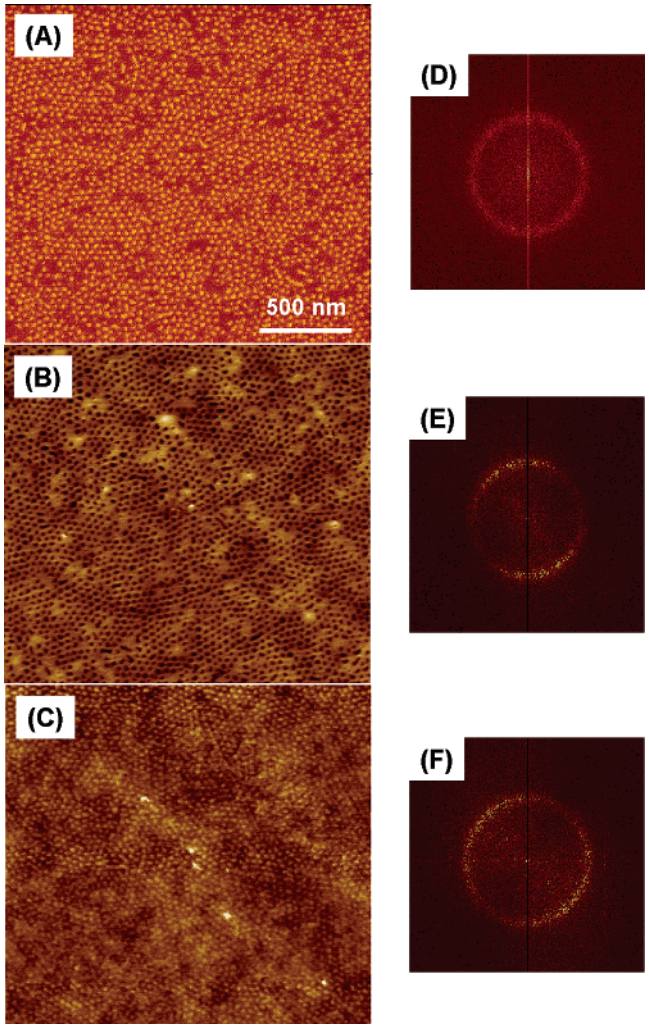

Figure 3. Height contrast AFM images of the surface of PS-*b*-PMMA/PMMA film for each step of the process to produce nanopore arrays as schematically illustrated in Figure 2: (A) topographic image of PS-*b*-PMMA/PMMA mixture film with an array of cylindrical PMMA nanodomains oriented normal to the substrate surface; (B) topographic image of the identical film after immersion in acetic acid; (C) topographic image of the identical film after immersion in acetic acid followed by annealing at 155 °C for 2 days under vacuum. The corresponding fast Fourier transform (FFT) images of the AFM images are displayed on the right side. The AFM images show a 2 μm × 2 μm area on the surface.

AFM image of the film surface after the film was immersed in acetic acid is shown in Figure 3B (corresponding to Figure 2B). A hexagonal array of nanopores (darker areas) in the PS matrix is observed across the entire film surface. The possible mechanism of pore formation by selective solvent swelling implies that PMMA homopolymers are extracted from the film while the PMMA blocks near the surface, tethered to the PS chains, are drawn to the film surface as schematically depicted in Figure 2B. Here, lateral expansion or compression of PS chains is unlikely since the PS matrix is a rigid glass at room temperature and acetic acid is a nonsolvent for PS. Comparing Figure 3A,B, one can see that the distribution of the PMMA domains of the film after selective solvent swelling (Figure 3B) is similar to that of the initial film (Figure 3A). The resulting film may contain nanopores of smaller diameters than the original cylindrical PMMA domains in Figure 3A, although it is difficult to quantify the precise lateral dimensions due to the tip convolution inherent in the AFM analysis. Shown in Figure 3C is the topographic AFM image after the nanoporous film (Figure 3B) was subjected to annealing at 155 °C (above T_g) for 2 days under vacuum. It is observed that the pores located at the film surface (Figure 3B) were covered with PMMA block chains. However, pores formed inside the film owing to the removal of PMMA homopolymer, originally present at the center of the cylindrical microdomains, were partially covered with PMMA block chains. Although these pores away from the top surface could not be discerned by the AFM analysis, OWS analysis described next clearly detected the existence of the nanopores in the resulting film.

Fast Fourier transforms (FFT) of the AFM images were obtained to investigate the lateral dimensions of the domain size. Comparison of the FFT images of the initial film (Figure 3D), the film treated with acetic acid (Figure 3E), and the film after reannealing (Figure 3F) confirms that the center-to-center distance between the cylinders (or the lattice periodicity) remains unchanged throughout the entire process. The λ_{C-C} was measured to be ~46 nm, providing evidence for the conservation of the lattice periodicity. This demonstrates that the lateral expansion of the film or compression of the PS chains did not occur due to the confinement of the film to the substrate.

We further investigated the surface morphologies of the film to demonstrate the presence of pores in the resulting film as well as the reversibility of this sequential swelling/annealing process. Figure 4 shows a series of AFM images of the film surfaces for each step of the repeated swelling/reannealing procedure. It is evident that ordered arrays of nanopores are observed as a result of the migration of PMMA block chains located on top of the closed pores onto the PS matrix after swelling and that the initial morphology is recovered after reannealing, indicating the reversibility of this process at the air/film interface. The surface morphology of the initial and resulting film was also compared with TEM images (See Figure S3 in the Supporting Information).

However, a question may still arise as to the presence or the shape of the pores inside the film after repeated swelling/annealing processes. To clarify this issue, a cross-sectional SEM image was taken from the film after the third swelling/reannealing step, and a typical side view of the fractured film was obtained as displayed in Figure 5. It is observed that the cylindrical pores in Figure 2B are broken up into multiple closed pores, resulting in a number of isometric or connected bubbles rather than continuous pores with a high aspect ratio. The central voids, which were initially occupied by the PMMA homopolymers, are partially filled by the PMMA block chains as a result of rearrangement and relaxation during the reannealing step.

The entire process discussed by microscopic measurements is analyzed by OWS as summarized in Figure 6. At first, we discuss the optical behavior of the initial PS-*b*-PMMA/PMMA film from the waveguide patterns (black curves) in Figure 6A,B, for *s*- and *p*-polarization, respectively, where characteristic transverse electric (TE) and transverse magnetic (TM) modes are observed. The best fits to the experimental curves (dashed curves) were also obtained based on Fresnel calculations to give the dielectric constant (ϵ) and film thickness (h), respectively. The decrease in the amplitude of the experimental data as compared with the calculated curves is attributed to the distribution in pore diameter and to the surface roughness of the film, which may disrupt the spatial coherence in the waveguide coupling conditions across the measured areas (~1 mm^2) corresponding to the laser beam size. The guided coupling modes of the BCP layer are entirely dictated by its effective dielectric constant (ϵ_{eff}) and its film thickness (h). The symmetry of the microdomain morphology, an array of cylinders with the

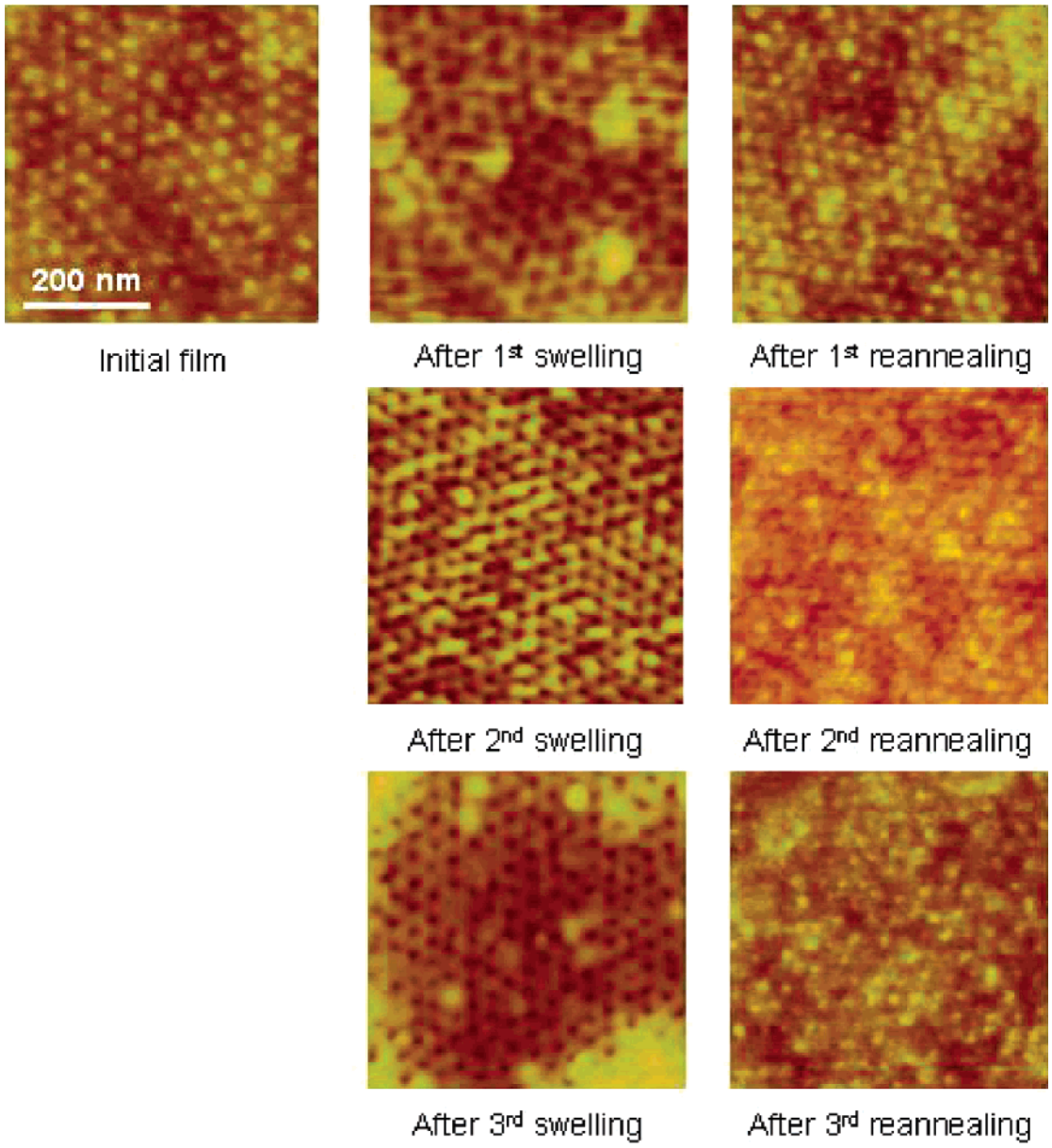

Figure 4. AFM images of the surfaces of a PS-*b*-PMMA/PMMA mixture film for each step of the repeated swelling/reannealing procedure. The film was treated with acetic acid for 30 min and annealed for 2 days, respectively, for each step of the swelling and annealing experiments. The AFM images show a 500 nm × 500 nm area on the surface.

axis aligned normal to the substrate surface, dictates that one of the principal axes of the dielectric function, $\epsilon_{\text{eff}} = \{\epsilon_x, \epsilon_y, \epsilon_z\}$, is parallel to the cylinder axis and that the two other ones are parallel to the film surface. As shown in Figure S2, the distribution of the cylindrical domains is isotropic, and a perfect hexagonal- packing is not observed. Thus, we assume $\epsilon_x = \epsilon_y$. Therefore, three parameters, ϵ_x ($= \epsilon_y$), ϵ_z, and h, need to be determined from the *s*- and *p*-polarized waveguide mode spectra. The values obtained from the fitting between experimental data and Fresnel calculations are $\epsilon_x = \epsilon_y = 2.405$, $\epsilon_z = 2.410$, in which the *z*-axis is the thickness direction of nanopore, and $h = 4644$ Å.

Next, the waveguide patterns of the BCP film for each step described in Figure 2A−C (or Figure 3A−C) are discussed. It is observed that the removal of the homo PMMA due to selective etching and swelling results in shifts in the coupling angles to lower values in both *s*- and *p*-polarization, respectively, which is characteristic of a decrease in the ϵ_{eff} (blue curves). The porosity of the film can be evaluated by comparing the experimental data and the theoretical calculation derived from the effective medium theory, using the following equations:.[35]

$$\epsilon_x = \epsilon_y = \epsilon_S + \frac{\epsilon_S f_D(\epsilon_D - \epsilon_S)\beta}{\epsilon_S - L f_D(\epsilon_D - \epsilon_S)\beta} \quad (1)$$

$$\epsilon_z = f_D\epsilon_D + f_S\epsilon_S \quad (2)$$

where f is the volume fraction, L is the source dyadic (1/2 in the case of the cylindrical microdomain), $\beta = 2\epsilon_S/(\epsilon_D + \epsilon_S)$, and D and S represent the cylindrical domain initially occupied by the PMMA (PMMA block and homo PMMA) and PS matrix, respectively. The ϵ_{PMMA} and ϵ_S values used in this study were 2.22 and 2.53, respectively.

The predicted patterns thus obtained (green curves), with the assumption that only the PMMA homopolymers were removed completely, are also shown in Figure 6. It is found that the coupling angles appear at lower angles than those of the experimentally observed patterns, indicating that sections of the

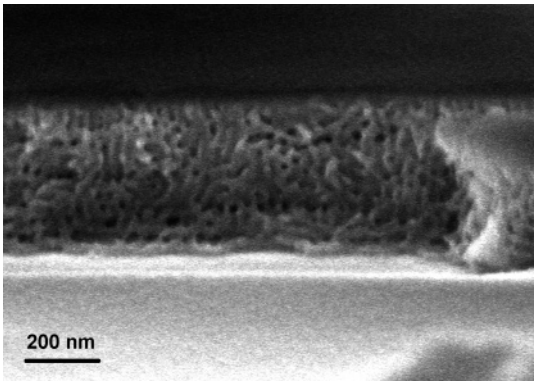

Figure 5. Typical cross-sectional SEM image of the PS-*b*-PMMA/PMMA mixture film after the third reannealing step. To enhance the contrast, whole PMMA chains were removed by exposing the film to UV followed by acetic acid rinsing. The SEM image of the identical film without UV treatment did not provide sufficient contrast where the minute pore domains were not clearly discerned (see Figure S4 in the Supporting Information).

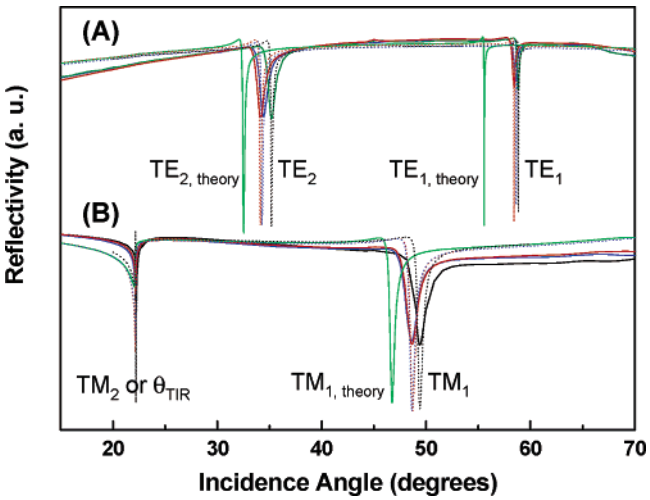

Figure 6. Waveguide mode patterns of the PS-*b*-PMMA/PMMA mixture film for each step of the process described in Figure 2 (or Figure 3) under *s*-polarization (A) and in *p*-polarization (B), respectively. The black, blue, and red curves indicate the waveguide patterns of the initial, swelled, and reannealed films, respectively. The dotted curves are the best fits to the respective experimental data. The green curve represents the hypothetical pattern obtained from the Fresnel calculation using ϵ values derived from the eqs 1 and 2, assuming that the PMMA homopolymers were completely removed by acetic acid treatment.

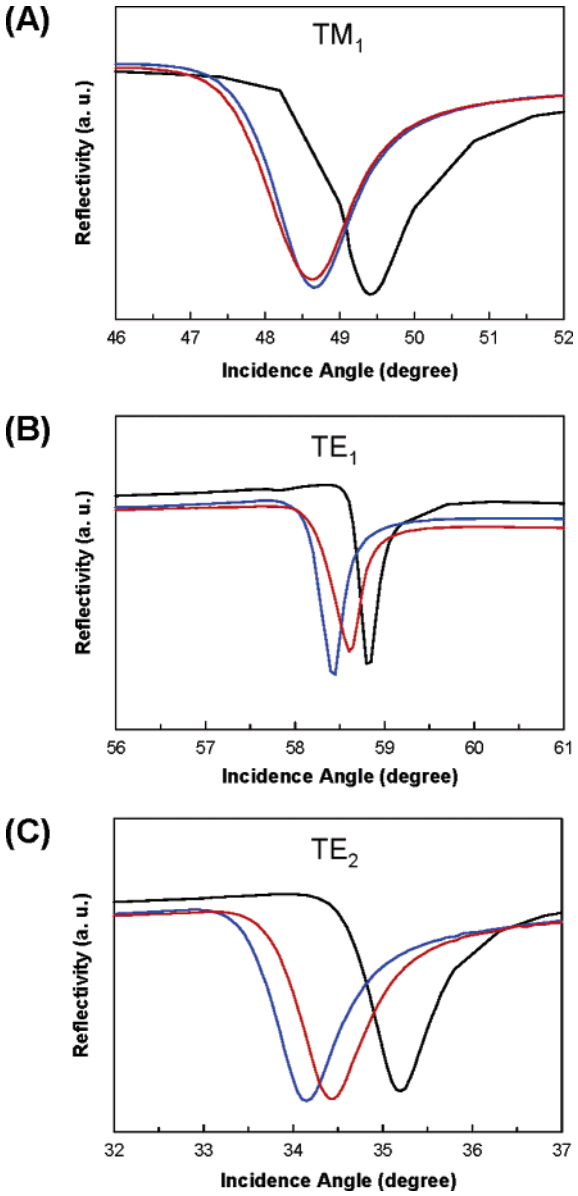

Figure 7. Guided optical modes of the waveguide patterns of the PS-*b*-PMMA/PMMA film for each step of the process depicted in Figure 4: (A) TM_1 mode under *p*-polarization; (B) TE_1 mode under *s*-polarization; and (C) TE_2 mode under *s*-polarization. The curves in black, blue, and red represent the initial film, the film after selective swelling with acetic acid, and the film after reannealing, respectively.

PMMA chains still remain after the acetic acid treatment. Comparison between the observed and the predicted patterns reveals that pores of ~5.4 vol % with respect to the total PMMA microdomains were generated in the resulting film, which is smaller than the fraction of the initial homo PMMA domains, 20.0 vol %, in the total PMMA microdomains. This discrepancy may be ascribed to several reasons including inherent limitations of the effective medium theory,[36,37] which better describes composites with a lower contrast of two dielectric constants rather than ones with higher contrasts, insufficient numbers of guided modes to allow for precise evaluation, and the mismatch of the beam spot on the sample surface during the ex situ experiment.[31] Also, a small value of the pore fraction obtained from OWS suggests that pores inside the film do not have a long-connection shape but have a string of closed pores, as shown schematically in Figure 2C.

The process during selective solvent swelling (blue curves) and reannealing (red curves) was further investigated using the respective guided optical modes. It is noted that the original film (black curves) exhibits two waveguide modes for each polarization (Figure 6). However, the TM_2 mode is convoluted with the critical angle due to total internal reflection (θ_{TIR}) and is not used for the analysis. Figure 7A shows the TM_1 mode for *p*-polarization, and Figure 7B,C display the TE_1 and TE_2 modes for *s*-polarization of the waveguide patterns of the PS-*b*-PMMA/PMMA film, respectively, for each step of the process that generates nanopores (as schematically depicted in Figure 2 and shown in the AFM images in Figure 3, respectively). The TM_1 mode was observed at $\theta = 49.40°$, while the TE_1 and TE_2 modes were observed at $\theta = 58.80°$ and $\theta = 35.20°$, respectively, for the initial BCP film (black curves). Selective etching and swelling with acetic acid resulted in the removal of the PMMA homopolymer and swelling of PMMA block chains. This was detected as shifts in the mode coupling angles to lower values (blue curves) (i.e., TM_1 to $\theta = 48.65°$ (Figure 7A), TE_1 to $\theta = 58.45°$ (Figure 7B), and TE_2 to $\theta = 34.15°$

(Figure 7C)), which is characteristic of a decrease in ϵ_{eff} (note that the dielectric constant of air, $\epsilon_{air} = 1.0$, is lower than that of PMMA, $\epsilon_{PMMA} = 2.220$). An interesting feature to note is that the angle shift for the TE_2 mode in Figure 7C, $\Delta\theta = 1.05°$, is higher than that for the TE_1 mode in Figure 7B, $\Delta\theta = 0.35°$. This effect is interpreted as a result of the thickness change due to the disappearance of the protrusion of the PMMA domains and the migration of the PMMA chains to the PS surfaces. This observation is consistent with the theory that any change in thickness results in asymmetric angle shifts (i.e., modes at lower angles shift more than those at higher angles).[38] The best fits to the experimental curves (dotted blue curves in Figure 6) give the dielectric constants, $\epsilon_x (= \epsilon_y) = 2.379$, and $\epsilon_z = 2.382$, for the selectively etched and swollen film.[39]

After reannealing above T_g (red curves), there is essentially no shift in the TM_1 mode (Figure 7A), while the TE_1 (Figure 7B) and TE_2 (Figure 7C) modes were shifted to higher angles as compared with the swollen film (blue curves) but still lower than those of the initial film (black curves). TM (transverse magnetic) waves have their electric fields oscillating parallel to the long cylinder/pore axis, thus probing the average composition of the film. In contrast, TE (transverse electric) waves oscillate parallel to the film plane. They interact strongly with the PS/PMMA and PS/air interface and are sensitive to changes in the domain/pore morphology. Therefore, the relative constancy of the TM_1 mode indicates no change in the average chemical composition after reannealing (i.e., the pore fraction essentially remains the same). However, the parallel shifts of the TE modes indicate a change in the optical density in the plane of the film. The PMMA chains tethered to the PS blocks, which migrated to the PS surface in the swelling step, restore the original configuration (i.e., protrusion from the PS surface) in the reannealing process. This was reflected by the shifts of the TE modes to higher angles, which were, however, lower than those of the original film, indicating that pores remain within the film. The dielectric constants and the film thickness of the reannealed film obtained from the fitting (dotted red curves in Figure 6) between experimental data and Fresnel calculations are as follows: $\epsilon_x (= \epsilon_y) = 2.384$, and $\epsilon_z = 2.384$.[39]

Thus, the complicated processes occurring simultaneously inside and on top of a thin film of a block copolymer/homopolymer mixture (i.e., pore formation and reversible migration of PMMA block chains) by selective solvent swelling and a subsequent reannealing process, which was not discerned by conventional microscopic analysis discussed in Figures 3 and 4, were successfully monitored by OWS.

Conclusion. Thin films composed of mixtures of asymmetric PS-*b*-PMMA diblock copolymers and PMMA homopolymers with cylindrical PMMA microdomains being oriented normal to the substrate surface were successfully used as waveguiding layers in an OWS study in the Kretschmann configuration. A typical process occurring in the BCP waveguide layer (i.e., nanopore formation as a result of selective solvent swelling for the minor PMMA domain and subsequent reannealing) was detected in terms of shifts in the coupling mode angles. Simultaneous processes occurring inside and on top of the BCP waveguide layer (i.e., pore formation and migration of the polymer chains to the film/air interface, respectively) were discerned independently for *p*- and *s*-polarization conditions. The dielectric constant (ϵ) of the BCP waveguide layer for each step (i.e., initial, swelled, and reannealed film) could be obtained from the best fit of the experimental data by Fresnel calculations using TM and TE waveguide modes. It has been found that a number of short or connected pores instead of continuous cylindrical pores with a high aspect ratio were generated inside the film, while a reversible migration behavior of the PMMA block chains was observed at the air/film interface, as a result of the repeated swelling/reannealing processes.

In summary, we presented a simple route to unprecedented nanoporous structures (i.e., arrays of capped pores with controllable volume fractions by a combined selective swelling and annealing) and verified the morphologies for each step of the fabrication process by AFM, TEM, FESEM, and OWS studies. On the basis of the methodology discussed in this work, complex events that can occur in nanoporous materials such as growth of one-dimensional nanomaterials inside or functionalization/adsorption on top of the BCP templates can be investigated by static or in situ kinetic mode OWS. Similar experimental strategies applied for porous aluminum oxide templates demonstrated the sub-angstrom sensitivity of OWS for such processes.[37] This work demonstrates the potential applications of BCP films in integrated optical devices[40] and suggests that OWS provides a significant advance over conventional analytical tools (e.g., microscopic or scattering methods) in terms of a cost-effective, simple home-built experimental setup and high sensitivity.

Acknowledgment. The authors are grateful to the financial support by the Deutsche Forschungemeinschaft (DFG) in the frame of a priority program, Schwerpunktprogramm 1165 (SPP 1165: KN 224/15-1). D.H.K. acknowledges the support of the Brain Korea 21 (BK21) program. T.P.R. acknowledges the support of the Department of Energy, Materials Science Division (DEFG0296ER45612). J.K.K. acknowledges the support of the Creative Research Initiative Program by the Korea Science and Engineering Foundation (KOSEF). C.J.H. acknowledges the support of the MRSEC Program of the National Science Foundation (UCSB MRL) under Award DMR05-20415.

Supporting Information Available: Scan mode SPR profiles from the coupling gap layers, Cr/Ag/3-MPS/SiO_2/P(S-*r*-MMA), deposited between the glass substrate and the block copolymer layer. Height contrast AFM image of the surface of PS-*b*-PMMA/PMMA mixture film fabricated on a P(S-*r*-MMA)/SiO_2/3-MPS/Ag/Cr/glass substrate with an array of cylindrical PMMA nanodomains oriented normal to the substrate surface in a 5 μm $\times$ 5 μm scale. TEM images of the surfaces of an initial ordered PS-*b*-PMMA/PMMA mixture film and the identical film after selective etching and swelling, followed by reannealing over the T_gs of the polymers. Typical cross-sectional SEM image of the PS-*b*-PMMA/PMMA mixture film after third reannealing step without UV treatment. This material is available free of charge via the Internet at http://pubs.acs.org.

References and Notes

(1) Hamley, I. W. *The Physics of Block Copolymers*; Oxford University Press: New York, 1998.

(2) Fredrickson, G. H.; Bates, F. S. *Annu. Rev. Mater. Sci*. **1996**, *26*, 501−550.

(3) Fasolka, M. J.; Mayes, A. M. *Annu. Rev. Mater. Res.* **2001**, *31*, 323−355.

(4) Hashimoto, T.; Shibayma, M.; Fujimura, M.; Kawai, H. *Block Copolymers, Science and Technology*; Meier, D. J., Ed.; Harwood Academic: London, 1983; pp 63−108.

(5) Muthukumar, M.; Ober, C. K.; Thomas, E. L. *Science* **1997**, *277*, 1225−1232.

(6) Lodge, T. P. *Macromol. Chem. Phys.* **2003**, *204*, 265−273.

(7) Lazzari, M.; López-Quintela, M. A. *Adv. Mater*. **2003**, *15*, 1583−1594.

(8) Hamley, I. W. *Angew. Chem., Int. Ed*. **2003**, *42*, 1692−1712.

(9) Hamley, I. W. *Nanotechnology* **2003**, *14*, R39−R54.
(10) Soler-Illia, G. J. de A. A.; Crepaldi, E. L.; Grosso, D.; Sanchez, C. *Curr. Opin. Colloid Interface Sci.* **2003**, *8*, 109−126.
(11) Förster, S.; Plantenberg, T. *Angew. Chem., Int. Ed.* **2002**, *41*, 688−714.
(12) Förster, S.; Konrad, M. *J. Mater. Chem.* **2003**, *13*, 2671−2688.
(13) Förster, S.; Antonietti, M. *Adv. Mater.* **1998**, *10*, 195−217.
(14) Park, C.; Yoon, J.; Thomas, E. L. *Polymer* **2003**, *44*, 6725−6760.
(15) Segalman, R. E. *Mater. Sci. Eng. R* **2005**, *48*, 191−226.
(16) Urbas, A. M.; Maldovan, M.; DeRege, P.; Thomas, E. L. *Adv. Mater.* **2002**, *14*, 1850−1853.
(17) Park, M.; Harrison, C.; Chaikin, P. M.; Register, R. A.; Adamson, D. H. *Science* **1997**, *276*, 1401−1404.
(18) Thurn-Albrecht, T.; Schotter, J.; Kästle, G. A.; Emley, N.; Shibauchi, T.; Krusin-Elbaum, L.; Guarini, K.; Black, C. T.; Tuominen, M. T.; Russell, T. P. *Science* **2000**, *290*, 2126−2129.
(19) Mansky, P.; Liu, Y.; Huang, E.; Russell, T. P.; Hawker, C. J. *Science* **1997**, *275*, 1458−1460.
(20) Thurn-Albrecht, T.; Steiner, R.; Derouchey, J.; Stafford, C. M.; Huang, E.; Bal, M.; Tuominen, M.; Hawker, C. J.; Russell, T. P. *Adv. Mater.* **2000**, *12*, 787−791.
(21) Jeong, U.; Ryu, D. Y.; Kho, D. H.; Lee, D. H.; Kim, J. K.; Russell, T. P. *Macromolecules* **2003**, *36*, 3626−3634.
(22) Jeong, U.; Kim, H. C.; Rodriguez, R. L.; Tsai, I. Y.; Stafford, C. M.; Kim, J. K.; Hawker, C. J.; Russell, T. P. *Adv. Mater.* **2002**, *14*, 274−276.
(23) Jeong, U.; Ryu, D. Y.; Kim, J. K.; Kim, D. H.; Wu, X.; Russell, T. P. *Macromolecules* **2003**, *36*, 10126−10129.
(24) Jeong, U.; Ryu, D. Y.; Kho, D. H.; Kim, J. K.; Goldbach, J. T.; Kim, D. H.; Russell, T. P. *Adv. Mater.* **2004**, *16*, 533−536.
(25) Xu, T.; Stevens, J.; Villa, J.; Goldbach, J. T.; Guarini, K. W.; Black, C. T.; Hawker, C. J.; Russell, T. P. *Adv. Funct. Mater.* **2003**, *13*, 698−702.
(26) Xu, T.; Goldbach, J. T.; Misner, M. J.; Kim, S.; Gibaud, A.; Gang, O.; Ocko, B.; Guarini, K. W.; Black, C. T.; Hawker, C. J.; Russell, T. P. *Macromolecules* **2004**, *37*, 2972−2977.
(27) Knoll, W. *Annu. Rev. Phys. Chem.* **1998**, *49*, 569−638.
(28) van Os, M. T.; Menges, B.; Förch, R.; Vancso, G. J.; Knoll, W. *Chem. Mater.* **1999**, *11*, 3252−3257.
(29) Chen, J. T.; Thomas, E. L.; Zimba, C. G.; Rabolt, J. F. *Macromolecules* **1995**, *28*, 5811−5818.
(30) Swalen, J. D. *J. Phys. Chem.***1979**, *83*, 1438−1445.
(31) Kim, D. H.; Lau, K. H. A.; Robertson, J. W. F.; Lee, O.-J.; Jeong, U.; Lee, J. I.; Hawker, C. J.; Russell, T. P.; Kim, J. K.; Knoll, W. *Adv. Mater.* **2005**, *17*, 2442−2446.
(32) Drockenmuller, E.; Li, L. Y. T.; Ryu, D. Y.; Harth, E.; Russell, T. P.; Kim, H.-C.; Hawker, C. J. *J. Polym. Sci., Polym. Chem.* **2005**, *43*, 1028−1037.
(33) Mansky, P.; Russell, T. P.; Hawker, C. J.; Pitsikalis, M.; Mayes, J. *Macromolecules* **1997**, *30*, 6810−6813.
(34) Thompson, W. R.; Cai, M.; Ho, M.; Pemberton, J. E. *Langmuir* **1997**, *13*, 2291−2302.
(35) Maldovan, M.; Bockstaller, M. R.; Thomas, E. L.; Carter, W. C. *Appl. Phys. B* **2003**, *76*, 877−884.
(36) Granqvist, C. G.; Hunderi, O. *Phys. Rev. B* **1978**, *18*, 2897−2906.
(37) Aspnes, D. E. *Thin Solid Films* **1982**, *89*, 249−262.
(38) Lau, K. H. A.; Tan, L.-S.; Tamada, K.; Sander, M. S.; Knoll, W. *J. Phys. Chem. B* **2004**, *108*, 10812−10818.
(39) The best fits were performed under a constraint of variable film thickness. However, reliable thickness values for each step of the process could not be drawn by these ex situ OWS measurements where different sample areas were probed for each step because the roughness of the evaporated underlying Au substrate was higher than the order of thickness changes involved in the swelling/annealing process.
(40) Ma, H.; Jen, A. K.-Y.; Dalton, L. R. *Adv. Mater.* **2002**, *14*, 1339−1365.